Inhibition of Premixed Methane Flames by Manganese and Tin Compounds[†]

GREGORY T. LINTERIS,* VADIM D. KNYAZEV,[a] and VALERI I. BABUSHOK

National Institute of Standards and Technology, Gaithersburg, MD 20899-8665, USA

The first experimental measurements of the influence of manganese- and tin-containing compounds (MMT, TMT) on the burning velocity of methane/air flames are presented. Comparisons with $Fe(CO)_5$ and CF_3Br demonstrate that manganese and tin-containing compounds are effective inhibitors. The inhibition efficiency of MMT is about a factor of two less than that of iron pentacarbonyl, and that of TMT is about 26 times less effective, although TMT is still about twice as effective as CF_3Br. There exist conditions for which both MMT and TMT show a loss of effectiveness beyond that expected because of radical depletion, and the cause is believed to be particle formation. Kinetic models describing the inhibition mechanisms of manganese- and tin-containing compounds are suggested. Simulations of MMT- and TMT-inhibited flames show reasonable agreement with experimental data. The decomposition of the parent molecule for the tin and manganese species is found to have a small effect on the inhibition properties for the concentrations in this work. The inhibition effect of TMT is determined mostly by the rate of the association reaction $H + SnO + M \leftrightarrow SnOH + M$, and the catalytic recombination cycle is completed by the reactions $SnOH + H \leftrightarrow SnO + H_2$ and $SnOH + OH \leftrightarrow SnO + H_2O$. The inhibition mechanism by manganese-containing compounds includes the reactions: $MnO + H_2O \leftrightarrow Mn(OH)_2$; $Mn(OH)_2 + H \leftrightarrow MnOH + H_2O$, and $MnOH + OH$ (or H) $\leftrightarrow MnO + H_2O$ (or H_2), and the burning velocity is most sensitive to the rate of the reaction $Mn(OH)_2 + H \leftrightarrow MnOH + H_2O$.   © 2002 by The Combustion Institute

INTRODUCTION

The production of the effective, bromine-based fire suppressants has been banned because of their ozone depletion potential, motivating a search for alternative compounds. Iron penta-carbonyl has been shown to be up to two orders of magnitude more effective than CF_3Br as a flame inhibitor; however, it loses its effectiveness because of condensation of the active species to particles. Consequently, it is of interest to determine if other metals cause similar strong flame inhibition while not suffering from the loss of effectiveness. Because manganese- and tin-containing species have higher vapor pressures than those of iron species, they are potential additives for fire suppression. The present work seeks to determine the gas-phase flame inhibition properties of tin and manganese through experiments and modeling of their influence on the premixed burning velocity of methane–air flames.

Metals have great potential as flame inhibitors because it is well known that they catalyze the recombination of radicals in the post combustion region of hydrogen–air flames [1–4]. For example, Bulewicz and Padley [1] demonstrated that metallic compounds of Cr, Mn, Sn, U, Mg, and Ba accelerate hydrogen atom recombination at ppm[1] levels. Nonetheless, careful studies of flame inhibition, with the goal of assessing the metals' effects on the overall reaction rate, are limited. Tin compounds are used as fire retardant additives for polymers, and to reduce smoke and CO formation [5, 6]. The mechanism of flame inhibition has been attributed to both the promotion of condensed phase char and gas-phase flame inhibition [6, 7]. Lask and Wagner [8] found $SnCl_4$ to be about 1/34 as effective as $Fe(CO)_5$ at reducing the burning velocity of premixed n-hexane–air flames by 30%, and Miller et al. [9] found it to be about 2/3 as effective as $Fe(CO)_5$ at reducing the flame speed of hydrogen-air flames by 80%. Miller [10] measured the amount of inhibitor required to lift-off a premixed $CH_4/O_2/N_2$ flat flame at low pressure, and found that tetra-

*Corresponding author. E-mail: linteris@nist.gov.

[†] Official contribution of NIST, not subject to copyright in the United States.

[a] Also at The Catholic University of America, Department of Chemistry, Washington, DC 20064.

[1]All references to ppm in the present paper are on a volume basis, and refer to μL/liter.

methyltin ($Sn(CH_3)_4$, TMT) and $SnCl_4$ required a mole fraction of 1.7% and 1.1%, respectively; whereas $Fe(CO)_5$ and Br_2 required 0.23% and 2.3%. Morrison and Scheller [11] investigated the effect of twenty flame inhibitors on the ignition of hydrocarbon mixtures by hot wires, and found that $SnCl_4$ was the most effective inhibitor tested for increasing the ignition temperature; whereas the powerful flame inhibitors CrO_2Cl_2 and $Fe(CO)_5$ had no effect on the ignition temperature. As a result of these studies, tin tetrachloride $SnCl_4$ was recommended as compound deserving further study [12].

The effects of manganese compounds on flames has also been studied. Vanpee and Shirodkar [13] investigated the influence of many metal chlorides and metal acetates and acetylacetonates on the limiting oxygen index at extinction in a partially premixed counterflow pool burner of ethanol and air. In their experiment, the inhibitor was dissolved in ethanol, which was aspirated into the air stream. They found manganese acetylacetonate to be more effective than acetylacetonates of iron or chromium. Westblom et al. [14] analyzed the consequence of trace amounts of methylcyclopentadienyl-manganese tricarbonyl ($CH_3C_5H_4Mn(CO)_3$, MMT) on the flame structure of a premixed propane–air flame at 5.33 kPa, but found no measurable effect. They suggested a kinetic model for the influence of MMT on those flames [14]. In a review article, Howard and Kausch [5] reported that manganese-containing compounds are among the most effective soot-reducing fuel additives. Finally, MMT is a known antiknock agent for gasoline [15], and Tapscott et al. [16] recently suggested manganese compounds as agents for further consideration in studies of fire suppression performance.

In this work we present data on flame inhibition by manganese- and tin-containing compounds. The additive influence was analyzed through the effects on the laminar burning velocity of methane-air mixtures for different equivalence ratios and oxygen mole fractions. The kinetic mechanisms of flame inhibition were analyzed by comparing simulation results with experimental data. The relative inhibition efficiency of TMT, MMT, $Fe(CO)_5$, and CF_3Br was deduced and analyzed. While the manganese and tin compounds tested are too toxic to

be used directly as fire suppressants, they provide convenient means for introducing Mn and Sn to a flame, so that the inhibition mechanisms of these elements can be studied.

EXPERIMENT

The laminar flame speed S_L provides a measure of an agent's reduction of the global reaction rate. While good techniques exist which allow measurement of burning velocity under conditions of controlled stretch rates [17], they require seeding with particles for determination of the local gas velocity. Because the presence of particles would influence the condensation rates of our metallic species, we instead employed the total area method with a Bunsen-type flame [18]. The experimental arrangement, described in detail previously [19–23], has been modified to accommodate new evaporators for TMT and MMT. A Mache-Hebra nozzle burner (1.0 cm $\pm$ 0.05 cm diameter) produces a premixed Bunsen-type flame about 1.3 cm tall with a straight-sided schlieren image that is captured by a video frame-grabber board in a PC. Digital mass flow controllers hold the oxygen mole fraction in the oxidizer stream $X_{O_2,ox}$, the equivalence ratio ϕ, and the flame height constant while maintaining the inlet mole fraction of the inhibitor (X_{in}) at the desired value. The average burning velocity is determined from the reactant flows and the schlieren image using the total area method. The fuel gas is methane (Matheson[2] UHP, 99.9%), and the oxidizer stream consists of nitrogen (boil-off from liquid N_2) and oxygen (MG Industries, H_2O less than 50 ppm, and total hydrocarbons less than 5 ppm). The inhibitors used are $Fe(CO)_5$ (Aldrich), TMT (Alfa Aesar), MMT (Alfa Aesar), CF_3Br (Great Lakes), N_2 (boil-off), and CO_2 (Airgas). The catalytic agents are liquids at laboratory conditions. Because they are required in low mole fraction, they are added to the flame in gaseous form rather than as drop-

---

[2]Certain commercial equipment, instruments, or materials are identified in this paper to adequately specify the procedure. Such identification does not imply recommendation or endorsement by the National Institute of Standards and Technology, nor does it imply that the materials or equipment are necessarily the best available for the intended use.

ϕ	$X_{O_2,ox}$	T_{in} K	T_{AFT} K	$S_{L,calc.}$ cm/s	$S_{L,exp}$ cm/s
TMT					
0.9	0.21	298	2159	35.3	33.9 ± 1.3
1.0	"	"	2235	39.6	38.0 ± 2.3
1.1	"	"	2193	39.8	38.0 ± 1.5
1.0	0.20	"	2185	34.7	33.6 ± 1.4
"	0.244	"	2377	57.0	58.0 ± 3.4
MMT					
0.9	0.21	353	2177	48.0	47.2 ± 1.5
1.0	"	"	2264	53.2	52.9 ± 2.9
1.1	"	"	2251	53.6	52.8 ± 2.0
1.0	0.19	"	2167	41.3	39.9 ± 1.6
"	0.2	"	2220	47.4	45.5 ± 1.7
"	0.244	"	2396	74.3	74.7 ± 4.1
MMT and Fe(CO)$_5$					
1.0	0.244	353	2396	74.3	75.9 ± 4.9

lets. The $Fe(CO)_5$ is added to the carrier gas using a two-stage saturator in an ice bath, described previously [21]. Nitrogen is the carrier gas for all agents. The TMT was added using an identical two-stage saturator, with a volume of liquid TMT in each stage greater than 50 cm^3 for all tests. The ice bath was maintained at (0 ± 0.2) °C with a maximum carrier gas flow 0.40 liter/min. Because of the toxicity of the agents, the $Fe(CO)_5$ and TMT saturators, as well as the premixed flame burner, were located in fume hoods. For the MMT, the saturator had three stages, each 20 cm long, 2.36 cm I.D. stainless steel tube, and the entire apparatus was submerged in a controlled temperature bath (Neslab), and vented. The bath temperature was typically (79.2 ± 0.1) °C, and the carrier gas flow for this saturator was always <0.5 liter/min. The mole fraction of the organometallic inhibitors in the air stream was calculated based on the measured air flow, measured carrier gas flow, and vapor pressure of the agent at the bath temperature, assuming saturated carrier gas. The parameters in the Antoine equation, $\log_{10}(P) = A-B/(T+C)$ (T in °C, P in bar), are (A,B,C): (6.77273, 4.0932, 7.2283), (1258.22, 1286.16, 1882), and (211.587, 235.846, 200) for $Fe(CO)_5$ [24], TMT [25], and MMT [26], respectively. Because the vapor pressure of MMT is much lower than that of the other agents,

experiments with MMT were conducted at a slightly elevated temperature, with the transfer lines and inlet gases maintained at (80 ± 3) °C and the burner tube maintained at (80 ± 1) °C. For the experiments with TMT and $Fe(CO)_5$, the inlet gas temperature T_{in} was (294.2 ± 1) K. Although the absolute value of the burning velocity is quite sensitive to the inlet temperature, comparisons of agent performance across this range of differing gas inlet temperatures is valid, since the *reduction* in the *normalized* burning velocity with agent addition is relatively insensitive in T_{in}. For example, calculations for inhibition by TMT (discussed below), and calculations and experiments with CO_2 (unpublished data of ref. [20]) show that changing the inlet gas temperature from 294 K to 353 K provides nearly identical curves of normalized burning velocity versus inhibitor mole fraction, differing from each other by less than 2% for the two inlet temperatures.

Tests were performed for a range of equivalence ratio and oxygen mole fraction in the oxidizer stream $X_{O_2,ox}$. The agent mole fraction is calculated relative to the total reactant flow. The test conditions are listed in Table 1. Note that while the inlet temperature for the $Fe(CO)_5$ and TMT experiments was 294 K, the experimental and numerically calculated burning velocities in the table have been converted

to equivalent values at 298 K to facilitate comparison with other values available in the literature.

The burning velocity in Bunsen-type flames is known to vary at the tip and base of the flame; however, these effects are most important over a small portion of the flame. We have taken several steps to minimize the influence of curvature and stretch on interpretation of the action of the chemical inhibitor. The nozzle burner produces visible and schlieren images which are very closely parallel. For the flame area, we use the schlieren image, which is maintained at a constant size (1.3 cm tall) for all tests. To reduce the error caused by flame curvature and stretch, we present the burning velocity of inhibited flames as a normalized parameter: the burning velocity of the inhibited flame divided by the burning velocity of the uninhibited flame. Also, we limit our interpretation of the data to inhibitor loading which produce less than 40% reduction in flame speed.

Determination of the uncertainties in the experimental data using the present apparatus has been described in detail previously [21]. For the present data, the uncertainty (expanded uncertainties with a coverage factor of 2) in the normalized burning velocity are less than ±5% for all cases. The uncertainty in the equivalence ratio is 1.4%. Neglecting the uncertainties (unspecified) in the vapor pressure correlation for $Fe(CO)_5$, TMT, and MMT, uncertainties in the bath temperature, ambient pressure and carrier gas flow rate yield an inhibitor mole fraction uncertainty of 6.5%.

KINETIC MECHANISMS AND NUMERICAL MODELING

There are few data on the chemical kinetics of tin compounds at flame temperatures, although kinetics studies of tin have been conducted for chemical vapor deposition. Studies with hydrogen-oxygen-nitrogen flames by Bulewicz and Padley [27] indicate that tin is present as Sn, SnO, and SnOH, with SnO overwhelmingly predominant. Recent spectroscopic data also indicate that tin is presents in flames as Sn, SnO, and SnOH [28], with SnO accounting for ~97% by volume of all tin species.

The present kinetic model for flame inhibi-

tion by tin compounds contains reactions of the species Sn, SnO_2, SnO, SnH, and SnOH. The reaction set is based on the consideration of possible reactions of tin-containing species with the radical pool and with the main species of methane combustion. The mechanism, listed in Table 2, consists of 37 reactions of tin-containing species. Rate constants were obtained from the literature when available, or otherwise estimated using empirical procedures and analogies with similar reactions. The reverse rates of the reactions in Table 2 are calculated from the forward rate and the equilibrium constant. It was assumed that tin (and manganese) species are non-reactive with hydrocarbon molecules. In the model development, estimates of rate constants were first made, and then the rates of the most important reactions were adjusted (based on sensitivity analysis) to provide agreement with the experimental results. The decomposition of TMT was described by the overall step listed in Table 2, but using the rate constant for the reaction $Sn(CH_3)_4 \rightarrow Sn(CH_3)_3 + CH_3$ [29]. Enthalpies of formation for the tin-containing (and manganese-containing) species are presented in Table 3. Enthalpies of formation for SnOH and SnH were estimated based on bond energies from refs. [27, 30].

The kinetic mechanism for studying the influence of manganese additives in premixed methane-air flames is presented in Table 4. The list of possible Mn-containing species participating in inhibition reactions includes Mn, MnH, MnO, MnOOH, MnHOH, MnOH, MnO, MnO_2, and $Mn(OH)_2$. All species except MnH and MnHOH were considered in the mechanism of Smith [31]. The role of MnOH and MnO in radical recombination was discussed by Bulewitz and Padley [1], and the species MnO and Mn were recently measured in a low pressure propane flame doped by MMT [14]. Hildenbrand and Lau [32] used mass spectrometry to identify the species MnO_2, MnOH, and $Mn(OH)_2$. We included the species MnH in the model since equilibrium calculations showed it to be present in significant quantities in MMT-inhibited flames. Transport parameters of tin- and manganese-containing species were estimated through analogy with similar metallic species, or based on molecular weight correlations for similar species.

TABLE 2

Kinetic mechanism for tin inhibition of premixed methane-air flames
($k = A\ T^b \exp(-E/RT)$, mole,s,cm,kJ)

No.	Reaction	A	b	E	Reference
1.	$SnC_4H_{12} \Rightarrow Sn+C_2H_6+C_2H_6$	7.94E+13	0.0	230.	[29]
2.	$Sn+H+M = SnH+M$	1.00E+15	0.0	0.0	e
3.	$Sn+OH+M = SnOH+M$	5.36E+18	−0.45	0.0	*
4.	$Sn+OH = SnO+H$	1.00E+13	0.0	27.2	e
5.	$Sn+O+M = SnO+M$	1.00E+17	0.0	0.0	e
6.	$Sn+O_2 = SnO+O$	3.07E11	0.79	3.63	[42]
7.	$Sn+O_2\ (+M) = SnO_2\ (+M)$	2.00E+13	0.0	0.0	e
	Low pressure limit:	1.5E+18	0.0	16.7	
8.	$Sn+HCO = SnH+CO$	3.00E+13	0.0	0.0	e
9.	$Sn+CH_3O = SnO+CH_3$	2.00E+13	0.0	0.0	e
10.	$Sn+CO_2 = SnO+CO$	1.39E+14	0.0	75.6	[42]
11.	$Sn+HO_2 = SnO+OH$	1.00E+13	0.0	0.0	e
12.	$SnO+H+M = SnOH+M$	5.50E+17	0.0	0.0	e
13.	$SnO+O+M = SnO_2+M$	1.00E+20	−1.0	0.0	e
14.	$SnO+HCO = SnOH+CO$	9.30E+13	0.0	0.0	e
15.	$SnO+HO_2 = SnOH+O_2$	3.00E+13	0.0	29.3	e
16.	$SnO_2+H = SnO+OH$	1.00E+14	0.0	8.37	e
17.	$SnO_2+OH = SnOH+O_2$	3.00E+12	0.0	31.4	e
18.	$SnO_2+OH = SnO+HO_2$	3.00E+12	0.0	46.0	e
19.	$SnO_2+O = SnO+O_2$	3.00E+13	0.0	8.37	e
20.	$SnO_2+CH3 = SnO+CH_3O$	3.00E+12	0.0	18.8	e
21.	$SnO_2+CO = SnO+CO_2$	2.00E+12	0.0	20.9	e
22.	$SnOH+H = Sn+H_2O$	1.20E+12	0.0	12.6	e
23.	$SnOH+H = SnO+H_2$	7.10E+13	0.0	4.18	e
24.	$SnOH+OH = SnO+H_2O$	6.30E+13	0.0	0.0	e
25.	$SnOH+O = SnO+OH$	3.00E+13	0.0	0.0	e
26.	$SnOH+O = SnO_2+H$	5.00E+12	0.0	37.7	e
27.	$SnOH+CH_3 = SnO+CH_4$	2.00E+13	0.0	4.18	e
28.	$SnH+H = Sn+H_2$	5.00E+13	0.0	4.18	e
29.	$SnH+OH = Sn+H_2O$	3.00E+13	0.0	0.0	e
30.	$SnH+OH = SnOH+H$	5.00E+12	0.0	20.9	e
31.	$SnH+O+M = SnOH+M$	1.00E+15	0.0	0.0	e
32.	$SnH+O = Sn+OH$	5.00E+13	0.0	4.18	e
33.	$SnH+O = SnO+H$	8.00E+12	0.0	4.18	e
34.	$SnH+CH_3 = CH_4+Sn$	5.00E+13	0.0	4.18	e
35.	$SnH+HCO = Sn+CH_2O$	2.00E+12	0.0	18.8	e
36.	$SnH+O_2 = SnO+OH$	3.00E+12	0.0	29.3	e

e Estimates.
  * By analogy with reactions of K species in Ref. [43]

For the manganese inhibition reaction set, we generated a list of ~160 reactions of Mn-containing species with the radical pool and with the main species of methane combustion. This list was reduced to 61 reactions based on thermochemical considerations and preliminary calculations. For the decomposition of MMT, we adopt the overall description suggested in ref. [14] and ref. [31], and use their rate constants for the Mn-species reactions whenever possible. Rate constants for the remaining reactions were estimated by analogy and based on thermochemical estimates. The main assumptions are the formation of MnO_2 through the reaction of Mn atom with oxygen molecule and the formation of $Mn(OH)_2$ via reaction of MnO with water (both by analogy to reactions of iron-containing species [33]).

Kinetic models for highly effective flame inhibitors can be considered to consist of two sub-models. The first sub-model includes reactions for the agent decomposition and formation of the active inhibiting species, and the second includes the inhibition reactions. In pre-

TABLE 3

Thermodynamic Properties for Tin- and Manganese-Containing Species (298.15 K)

Species	Enthalpy of Formation kJ/mol	Entropy J/(mol K)	Heat Capacity J/(mol K)	Ref.
Mn	283.6	173.6	20.8	[44]
MnO	161.7	236.0	31.7	[44]
MnO_2	23.01	269.3	42.2	[44]
MnOH	17.32	250.3	45.8	[44]
$Mn(OH)_2$	−373.2	291.2	67.1	e, [31]
MnOOH	−116.3	283.3	53.9	e, [31]
MnH	197.9	213.6	29.6	[44]
MMT	−439.3	401.7	149.9	[31]
Sn	301.2	168.4	21.3	[44]
SnO	21.91	232.1	31.8	[44]
SnO_2	11.69	251.5	49.5	[44]
SnOH	−15.06	244.8	46.0	e, [27]
SnH	268.2	214.7	29.7	e, [30]
$Sn(CH_3)_4$	−17.70	361.2	137.8	[45], [46]
Sn_2	425.4	267.2	42.1	[44]

e Estimation.

vious work, it has been shown that for the phosphorus-containing compound DMMP and for ferrocene, the decomposition reactions have a small influence on the predicted inhibitor efficiency as long as the overall activation energy of decomposition is less than 250 to 335 kJ/mol [20, 34]. In the present work, this was also found to be true for TMT and MMT decomposition.

The laboratory flames inhibited by TMT and MMT were numerically modeled as one-dimensional freely propagating flames. Solutions were obtained using the Sandia flame code *Premix* [35], and the *Chemkin* [36] and transport property [37] subroutines (solutions were obtained for values of GRAD and CURV of 0.17 and 0.25 in PREMIX). The kinetic mechanism for methane combustion was GRIMech 3.0 [38], with the nitrogen chemistry removed. The methane sub-mechanism contains 36 species and 219 reactions. It should be emphasized that the reaction mechanisms used for the present calculations for flames with manganese or tin compounds should be considered only as a starting point. Numerous changes to both the rates and the reactions incorporated may be made once a variety of experimental and theoretical data are available for testing the mechanism. Note also that the calculations are for 1-D planar flames, while the experiments determine the average flame speed of Bunsen-type flames

which can be influenced by curvature and stretch. To minimize these effects, both the experimental and calculated data are presented as normalized flame speed reduction.

RESULTS

Observations

The appearance of the flames with added organometallic inhibitors is shown in Fig. 1. Flames with iron pentacarbonyl are bright orange, with tetramethyltin they are bright pale blue, and with MMT, yellow-green. The intensity of the visible emission increases with inhibitor mole fraction. As the loading of metallic inhibitor increases, there becomes visible a luminous outer shroud as seen clearly in the last two images on the right in Fig. 1. We believe these are regions of high particle concentration from inhibitor condensation, leading to broad-band black body radiation, visible here in the orange part of the spectrum. For the TMT-inhibited flames, a white-colored powder (presumably tin oxide) formed on the rim of the quartz burner tube during the tests, especially at high TMT loading. This deposit was removed between collection of each data point. For MMT and $Fe(CO)_5$, a dark red or an orange deposit was

TABLE 4

Kinetic Mechanism for Manganese Inhibition of Premixed Methane-Air Flames
($k = A\, T^b \exp(-E/RT)$, mole,cm,s,kJ)

No.	Reaction	A	b	E	Reference
1.	$Mn+H+M = MnH+M$	1.00E+15	0.0	0.0	e
2.	$Mn+OH+M = MnOH+M$	8.00E+22	−2.2	0.0	[31]
3.	$Mn+O+M = MnO+M$	1.00E+15	0.0	0.0	e
4.	$Mn+O_2 = MnO+O$	2.50E+14	0.0	125.5	[31]
5.	$Mn+O_2 (+M) = MnO_2 (+M)$	2.00E+13	0.0	0.0	e
	Low pressure limit:	1.5000E+18	0.0	12.6	
6.	$Mn+HCO = MnH+CO$	3.00E+13	0.0	0.0	e
7.	$MnO+H+M = MnOH+M$	7.00E+15	0.0	0.0	[31]
8.	$MnO+O+M = MnO_2+M$	2.00E+19	−1.0	0.0	[31]
9.	$MnO+H = Mn+OH$	1.00E+14	0.0	16.7	e
10.	$MnO+OH+M = MnOOH+M$	3.00E+17	0.0	0.0	e
11.	$MnO+CH_3 = Mn+CH_3O$	1.00E+14	0.0	29.3	e
12.	$MnO+H_2 = Mn+H_2O$	3.00E+12	0.0	20.9	[47]
13.	$MnO+H_2O = MnO_2H_2$	5.40E+12	0.0	0.0	[47]
14.	$MnO+CO = Mn+CO_2$	3.00E+11	0.0	0.0	[31]
15.	$MnO+HCO = MnOH+CO$	2.40E+13	0.0	0.0	[31]
16.	$MnO+CH_2OH = MnOH+CH_2O$	2.40E+13	0.0	0.0	[31]
17.	$MnO_2+H+M = MnOOH+M$	2.00E+22	−1.5	0.0	[31]
18.	$MnO_2+H = MnO+OH$	1.00E+14	0.0	29.3	e
19.	$MnO_2+OH = MnOH+O_2$	3.00E+12	0.0	29.3	e
20.	$MnO_2+O = MnO+O_2$	5.00E+13	0.0	8.37	e
21.	$MnO_2+CO = MnO+CO_2$	2.00E+12	0.0	20.9	e
22.	$MnOH+H = Mn+H_2O$	1.20E+12	0.0	2.09	[31]
23.	$MnOH+H = MnO+H_2$	3.00E+13	0.0	4.18	e
24.	$MnOH+OH+M = MnO_2H_2+M$	1.00E+23	−2.0	0.0	[31]
25.	$MnOH+OH = MnO+H_2O$	1.00E+13	0.0	6.28	[31]
26.	$MnOH+O+M = MnOOH+M$	1.00E+18	0.0	0.0	e
27.	$MnOH+O = Mn+HO_2$	3.00E+13	0.0	71.1	e
28.	$MnOH+O = MnO+OH$	3.00E+13	0.0	0.0	[31]
29.	$MnOH+O = MnO_2+H$	5.00E+12	0.0	37.7	e
30.	$MnOH+CH_3 = MnO+CH_4$	2.00E+13	0.0	12.6	e
31.	$MnOOH+H+M = MnO_2H_2+M$	1.00E+16	0.0	0.0	e
32.	$MnOOH+H = MnO+H_2O$	2.00E+13	0.0	0.0	e
33.	$MnOOH+H = MnOH+OH$	3.00E+13	0.0	20.9	e
34.	$MnOOH+H = MnO_2+H_2$	1.00E+13	0.0	16.7	e
35.	$MnOOH+OH = MnO_2+H_2O$	6.00E+12	0.0	6.28	[31]
36.	$MnOOH+O = MnOH+O_2$	2.00E+13	0.0	10.5	e
37.	$MnOOH+O = MnO+HO_2$	3.00E+12	0.0	66.9	e
38.	$MnOOH+O = MnO_2+OH$	3.00E+13	0.0	18.8	e
39.	$MnOOH+CH_3 = MnO+CH_3OH$	3.00E+12	0.0	31.4	e
40.	$MnOOH+CH_3 = MnOH+CH_3O$	1.00E+13	0.0	46.0	e
41.	$MnOOH+CO = MnOH+CO_2$	2.00E+12	0.0	20.9	e
42.	$MnO_2H_2+H = MnOH+H_2O$	6.60E+13	0.0	4.18	e
43.	$MnO_2H_2+H = MnOOH+H_2$	5.00E+13	0.0	79.5	e
44.	$MnO_2H_2+OH = MnOOH+H_2O$	1.00E+13	0.0	37.7	e
45.	$MnO_2H_2+O = MnOOH+OH$	2.00E+13	0.0	83.7	e
46.	$MnO_2H_2+CH_3 = MnOOH+CH_4$	1.00E+13	0.0	87.9	e
47.	$MnH+H = Mn+H_2$	5.00E+13	0.0	12.6	e
48.	$MnH+OH = Mn+H_2O$	1.00E+14	0.0	0.0	e
49.	$MnH+O+M = MnOH+M$	1.00E+15	0.0	0.0	e
50.	$MnH+O = Mn+OH$	1.00E+14	0.0	8.37	e
51.	$MnH+CH_3 = CH_4+Mn$	1.00E+14	0.0	8.37	e
52.	$MnH+O_2+M = MnOOH+M$	1.00E+16	0.0	0.0	e

e Estimates.

Fig. 1. Visible image of methane-air premixed flame (from left to right: no inhibitor, 50 ppm of Fe(CO)$_5$, 4000 ppm of TMT, and 400 ppm of MMT).

formed, respectively. The rate of deposition for these inhibitors, however, was much lower than for the TMT, which was added to the flames at mole fractions about ten times higher.

Inhibition by Tetramethyltin

Fig. 2 shows the relative burning velocity reduction with addition of TMT to methane-air flames ($X_{O_2,ox}$, = 0.21) for values of equivalence ratio of 0.9, 1.0, and 1.1. The dotted lines are curve fits to the experimental data, and the solid lines are the results of the numerical calculations described above (and discussed below). Data are plotted as normalized burning velocity, which is the burning velocity of the inhibited flame divided by the value for the same flame in

Fig. 2. Normalized burning velocity of premixed CH$_4$/O$_2$/N$_2$ flames inhibited by TMT with $X_{O_2,ox}$ = 0.21 and ϕ = 0.9, 1.0, and 1.1 (dotted lines: curve fits to data; solid lines: numerical predictions).

the absence of inhibitor. The calculated and experimental burning velocities, along with the calculated adiabatic flame temperatures of the uninhibited flames used for the normalization are listed in Table 1. For the uninhibited flames, the experimentally determined average burning velocities for the Bunsen-type flames are within about 4% of the calculated values for 1-D planar flames. The experimental results in Fig. 2 demonstrate that for stoichiometric flames, 3000 ppm of TMT reduces the flame speed by about 41%, which is about a factor of two better than CF$_3$Br. The data also show that, unlike Fe(CO)$_5$, the richer flames are inhibited more strongly by TMT than the leaner flames. (Additional numerical tests with SnO as the inhibitor showed that the poorer inhibition of lean flames was because of the fuel effect from the hydrocarbon portion of the relatively large amounts of Sn(CH$_3$)$_4$ added to the flames.)

As described below, the burning velocity reduction caused by tin species is most sensitive to the rates of the reactions: SnO + H + M $\leftrightarrow$ SnOH + M, and SnOH +H $\leftrightarrow$ SnO + H$_2$. Consequently, we adjusted the pre-exponential factor in those rates to provide agreement with the experimental results for stoichiometric mixtures of methane with air. Note, however, the relatively high level of the rate constant for the reaction H + SnO + M $\leftrightarrow$ SnOH + M. Bulewicz and Padley [1] also found that a high rate was required for this process to provide agreement with their experimental data on hydrogen atom recombination in the products of a hydrogen flames. As Fig. 2 shows, the numerical model predicts the amount of inhibition well for stoichiometric flames. For rich and lean flames,
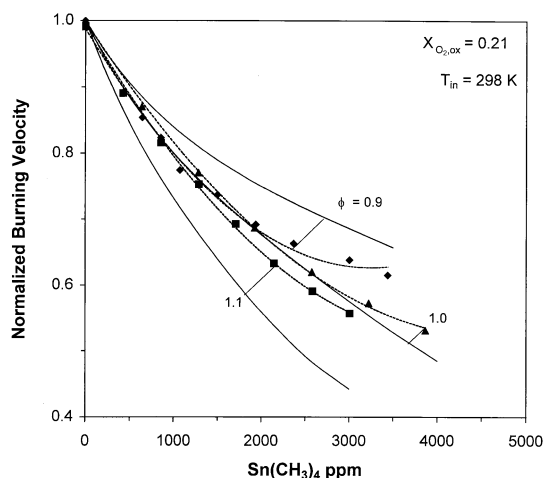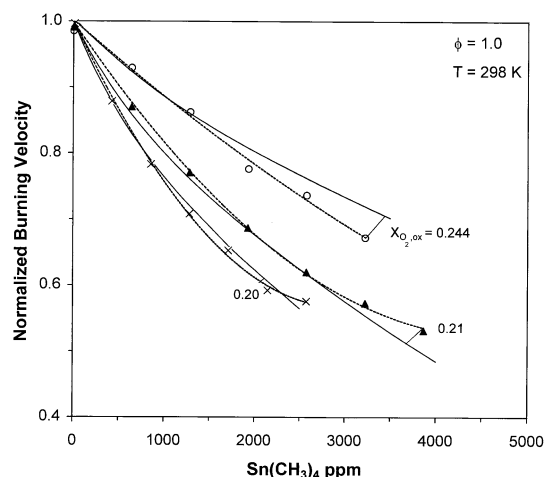
Fig. 3. Normalized burning velocity of premixed $CH_4/O_2/N_2$ flames inhibited by TMT, with $\phi = 1.0$ and $X_{O_2,ox} = 0.20$. 0.21, and 0.244 (dotted lines: curve fits to the data; solid lines: numerical predictions).
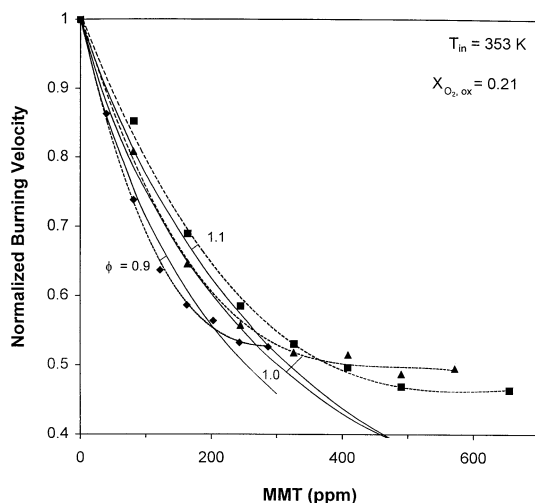

Fig. 4. Normalized burning velocity of premixed $CH_4/O_2/N_2$ flames inhibited by MMT with $X_{O_2,ox} = 0.21$ and $\phi = 0.9$, 1.0, and 1.1 (dotted lines: curve fits to data; solid lines: numerical predictions).

however, the model over- and under-predicts the burning velocity, respectively. We attempted to adjust the rates of reactions with tin species to improve the model performance for rich and lean flames. For the reaction set considered, we were not able to find reasonable adjustments to the rate constants to provide better agreement.

Figure 3 shows the measured and calculated flame speeds for TMT in stoichiometric flames $X_{O_2,ox}$, equal to 0.20, 0.21, and 0.244. The experimental data and calculations (with adjusted rate constants) show good agreement for the three values of $X_{O_2,ox}$; however, for the hottest flames ($X_{O_2,ox} = 0.244$) the mechanism slightly overpredicts the inhibition at low mole fraction, and underpredicts it for higher mole fraction. The experimental data show that for the slower and cooler flames (e.g., equivalence ratio is 0.9 or 1.0 and $X_{O_2,ox} = 0.20$ or 0.21), the TMT starts to lose its effectiveness above a certain value. For $Fe(CO)_5$ inhibited flames, such behavior was shown to be because of condensation of the iron-containing intermediates [22]).

Inhibition by MMT

The premixed flames inhibited by manganese-containing compound MMT were slightly pre-heated ($T_{in} = 80°C$). The values of the calcu-

lated and experimental uninhibited burning velocities, and the adiabatic flame temperatures are shown in Table 1. The normalized burning velocities of MMT-inhibited flames with variation in equivalence ratio and $X_{O_2,ox}$ are shown in Fig. 4 and Fig. 5. MMT is seen to be about thirteen times more efficient at flame inhibition than TMT; however, it too starts to lose its effectiveness for flame speed reductions near
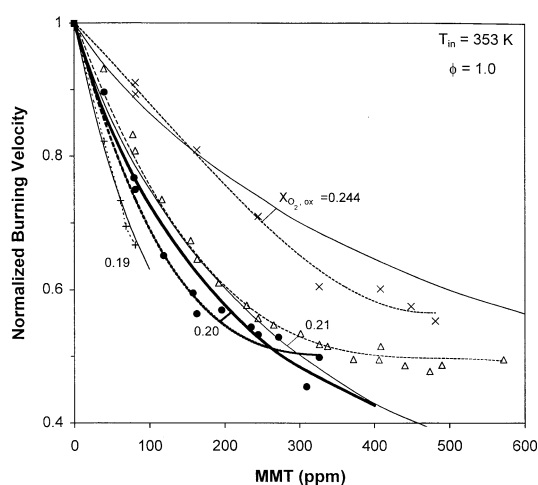

Fig. 5. Normalized burning velocity of premixed $CH_4/O_2/N_2$ flames inhibited by MMT, with $\phi = 1.0$ and $X_{O_2,ox} = 0.19$, 0.20. 0.21, and 0.244 (dotted lines: curve fits to the data; solid lines: numerical predictions).
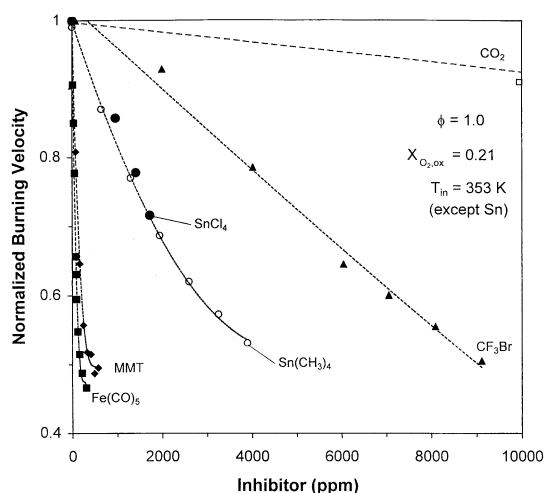
Fig. 6. Normalized burning velocity of premixed $CH_4/O_2/N_2$ flames inhibited by CO_2, CF_3Br, $Sn(CH_3)_4$, $SnCl_4$ [8], MMT, and $Fe(CO)_5$ (T_{in} = 353 K for all data except $Sn(CH_3)_4$ and $SnCl_4$ which are at 298 K). Lines are curve fits to data.

50%. Based on the sensitivity of the burning velocity to the reaction rates, we adjusted the pre-exponential factors of the reactions $Mn(OH)_2 + H \leftrightarrow MnOH + H_2O$, and $MnO + H_2O \leftrightarrow Mn(OH)_2$ to provide agreement with our experimental data for these methane-air flames at ϕ = 1.0. Using the rates shown in Table 4, the model predicts the burning velocity reduction quite well. Nonetheless, for the hottest flames ($X_{O_2,ox}$ = 0.244) this mechanism also overpredicts the inhibition slightly at low inhibitor mole fraction, and underpredicts the inhibition somewhat at intermediate mole fractions. Also, this gas-phase mechanism does not capture the decrease in inhibitor effectiveness which occurs with increasing inhibitor initial mole fraction, likely a result of condensation of Mn-containing species.

Comparative Performance

Figure 6 compares the inhibition effectiveness of $Fe(CO)_5$, MMT, TMT, $SnCl_4$, CF_3Br, and CO_2. The data for $SnCl_4$ inhibition from ref. [8] show tin tetrachloride to be as effective in n-hexane/air flames as TMT is in methane/air flames. Although the experimental data for TMT and $SnCl_4$ are not for an elevated inlet temperature of 80°C, numerical calculations indicate that the reduction in the

normalized flame speed caused by TMT addition with T_{in} = 298 K differs from that with T_{in} = 353 K by less than 1%. $Fe(CO)_5$ is significantly more effective than any of the other agents, and all of the metal-based inhibitors appear to have greatly reduced effectiveness for burning velocity reductions greater than 50%. If the inhibitor mole fractions are re-scaled in Fig. 6 to provide overlap at 30% reduction in burning velocity, the normalized burning velocity curves of all inhibitors are nearly coincident for flame speed reductions less than 40% (i.e., the curves are roughly linear up to this amount of normalized flame speed reduction). Such re-scaling of the experimental data shows that at low mole fraction, $Fe(CO)_5$ is about eighty times, MMT forty times, and TMT three times as effective as CF_3Br at reducing the overall reaction rate of stoichiometric, premixed methane-air flames. For flame speed reductions greater than 40%, the curves for these five agents diverge. As discussed previously [39,40], most inhibitors lose their marginal effectiveness at higher mole fractions, but the decrease of inhibition effectiveness is much more dramatic for the organometallic compounds (as found previously for $Fe(CO)_5$).

Blends of Agents

One approach for overcoming the loss of effectiveness is to add non-condensing amounts of several inhibitors. To test this approach in premixed flames, we performed tests with a blend of MMT and $Fe(CO)_5$, added at a molar ratio of 2:1, respectively. Data for pure MMT, pure $Fe(CO)_5$, and their combination are shown in Fig. 7 (T_{in} = 353 K, ϕ = 1.0, and $X_{O_2,ox}$ = 0.244). The experimental data are represented by the points with a curve fit (dotted line), while the results of the numerical calculations are shown by the solid lines. (The data for the combination of MMT and $Fe(CO)_5$ are plotted as a function of the mole fraction of the abundant agent, MMT.) The numerical model, which includes both the reactions of manganese-containing species and the iron-containing species from Ref. [33] predicts well the normalized flame speed reduction. As the figure shows, adding 0.5 moles of $Fe(CO)_5$ for each mole of MMT added does provide additional flame speed reduction over that from MMT alone. This is significant since, as discussed previously
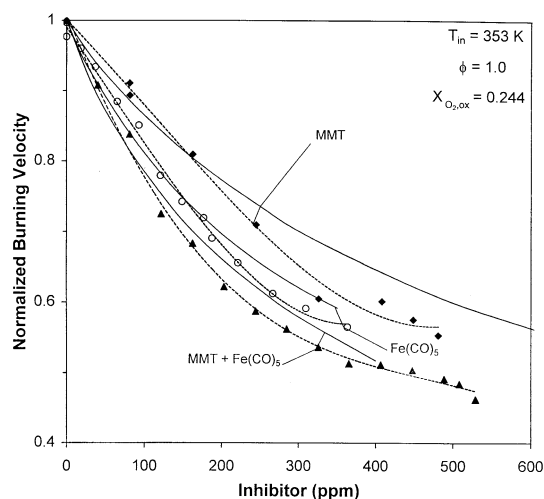
Fig. 7. Normalized burning velocity of premixed $CH_4/O_2/N_2$ flames inhibited by pure MMT and $Fe(CO)_5$, and by a blend of the two (dotted lines are curve fits to the data; solid lines are numerical model calculations).

[22], the loss of effectiveness of the metals at higher concentration could be caused either by condensation of active species, or by the loss of radical population by catalytic recombination. Since the addition of iron to the manganese-inhibited flame causes significant additional inhibition, the *strong* loss of effectiveness in the MMT-inhibited flames is likely because of condensation rather than radical depletion. If the cause was radical depletion, addition of $Fe(CO)_5$ to the flames already inhibited by high amounts of MMT would yield no additional inhibition, since few radicals would be left to recombine. The gas-phase kinetic model captures the *mild* reduction of effectiveness of either agent or their blend acceptably well (for flame speed reductions of less than 40%).

DISCUSSION

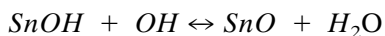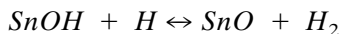### Inhibition Mechanisms of Tin and Manganese

Examination of species profiles, reaction fluxes, and sensitivity coefficients from the numerically predicted flame structure allows investigation of the mechanisms of inhibition of these metallic compounds. The calculations show that TMT decomposes quickly in the flame, with 90%

consumption at 1000 K. A diagram showing the important reactions for tin inhibition is shown in Fig. 8 (which also shows in parallel format the reaction paths for MMT and $Fe(CO)_5$ inhibition). In the calculations used to prepare Fig. 8, TMT, MMT, or $Fe(CO)_5$ were present at (1963, 128, or 105) ppm, respectively, in the premixed methane-air flames ($\phi = 1.0$, $T_{in} = 353$ K, and $X_{O_2,ox} = 0.21$); these volume fractions produced a 30% reduction in flame speed. The determination of the important reactions was based on consideration of both the reaction flux and sensitivities. The reaction flux represents the production or consumption of a species by chemical reaction. For a particular reaction, it is defined as the integral that reaction rate per unit volume over the entire flame domain. The total reaction flux for a species is defined as the sum of the reaction fluxes for the individual reactions which produce or consume it. In Fig. 8, the pathway for consumption of each species is shown, with arrows connecting the relevant reactant and product species. The number next to each arrow represents the fraction of the total consumption flux for that species which proceeds through that particular reaction.

The tin atom formed as a result of TMT decomposition quickly reacts with O_2 through the reactions $Sn + O_2 (+M) \leftrightarrow SnO_2$, and $Sn + O_2 \leftrightarrow SnO + O$. The former reaction leads to SnO from the reaction of SnO_2 with CO, H, or other radicals. Conversely, the latter reaction forms SnO directly, and is fast at room temperature as compared to the analogous reaction of iron atom. Formation of SnO leads to the following reactions with H and HCO radicals:

$$SnO + H + M \leftrightarrow SnOH + M$$
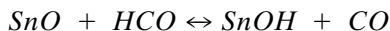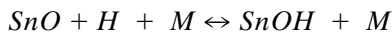
$$SnO + HCO \leftrightarrow SnOH + CO$$

which, together with the radical scavenging reactions of SnOH, complete the catalytic radical recombination cycle of tin:

$$SnOH + H \leftrightarrow SnO + H_2$$

$$SnOH + OH \leftrightarrow SnO + H_2O$$

$$SnOH + CH_3 \leftrightarrow SnO + CH_4$$
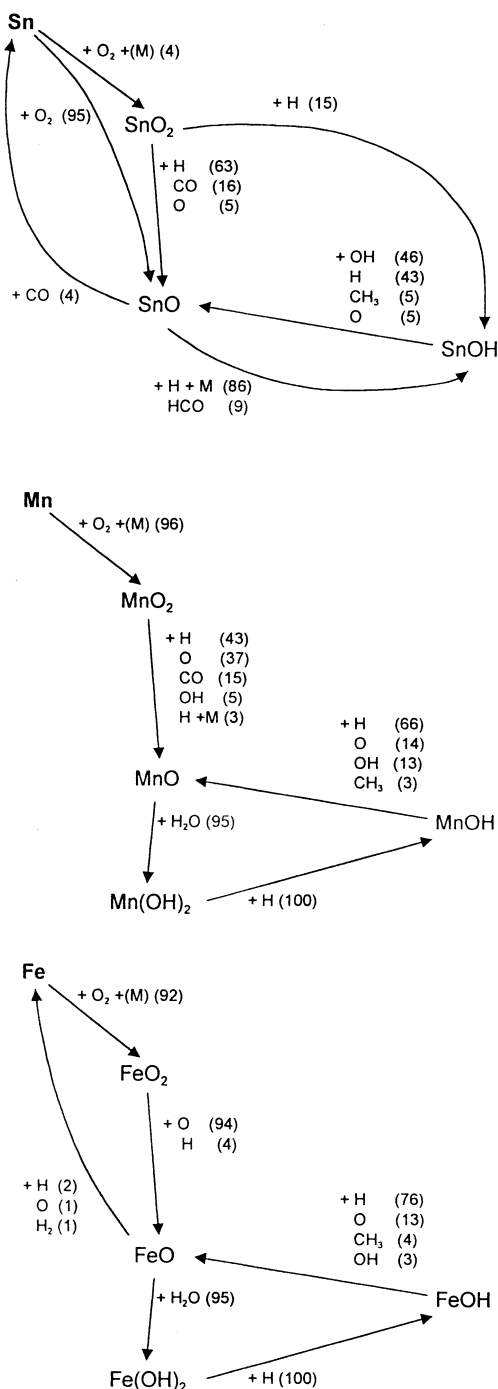
$$SnOH + O \leftrightarrow SnO + OH.$$
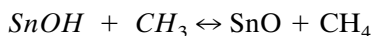
Fig. 8. Reaction pathway for Sn, Mn, and Fe in a premixed methane-air flame ($\phi = 1.0$, $X_{O_2,ox} = 0.21$, $T_{in} = 353$ K). TMT, MMT, and Fe(CO)$_5$ present at (1963, 128, or 105) ppm, respectively. The numbers in parentheses are the fractional consumption (percent) of the reactant molecule to a specific product, via reaction with the species in question.

The net effect of the dominant inhibition reactions can be shown as:

$$SnO + H + M \leftrightarrow SnOH + M$$

$$SnOH + H \leftrightarrow SnO + H_2$$

$$\overline{net: H + H \leftrightarrow H2}$$
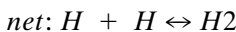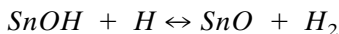
Equilibrium calculations show that SnO is the major tin species in the products of a stoichiometric methane–air flame with added TMT.

Figure 9 presents the sensitivity coefficients of the burning velocity to the rate constants (after adjustment) of tin-containing species for methane/air mixtures with equivalence ratios of 0.9, 1.0, and 1.1. In general, the burning velocity is sensitive to the rates of the catalytic cycle reactions with high fluxes: SnO reaction with H or HCO, and SnOH reaction with H, OH, CH$_3$, or O. The burning velocity is most sensitive to the rate of the reaction SnO + H + M $\leftrightarrow$ SnOH + M, which has a sensitivity about four times less than the chain-branching reaction H + O$_2$ $\leftrightarrow$ OH + O. As was found for DMMP and ferrocene additives [20, 34], the burning velocity of flames inhibited by TMT is not particularly sensitive to the rate of the decomposition reaction. Numerical tests showed that changes in the overall activation energy of TMT decomposition in the range 170 kJ/mol to 335 kJ/mol have little effect on the burning velocity with up to 2000 ppm of TMT. Hence, the inhibition effectiveness of tin compounds is likely to be independent on the parent molecule, as long as rapid decomposition occurs.

The reaction SnO + CO $\leftrightarrow$ Sn + CO$_2$ (which is followed by Sn+O$_2$ = SnO+O) is an additional route for CO consumption, and is chain-branching (net: CO+O$_2$ = CO$_2$+O), which reduces the inhibiting effect of SnO in these flames. Similar behavior was found for CO–N$_2$O flames inhibited by Fe(CO)$_5$ [41]. Changes in these rates affect the calculated inhibition efficiency of TMT; nevertheless, the mechanism is dominated by the rate of reaction SnO + H + M $\leftrightarrow$ SnOH + M.

Analysis of the numerical results for inhibition by MMT shows that the behavior of manganese in premixed methane-air flames is similar in many details to that of iron pentacarbonyl.
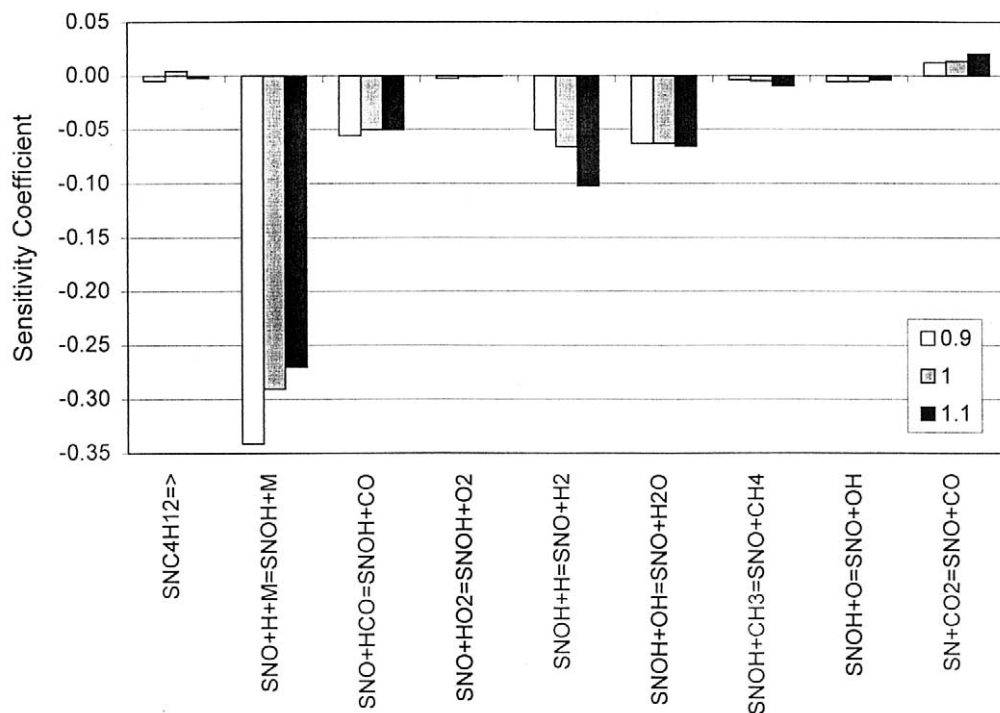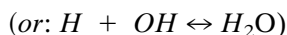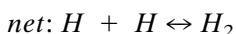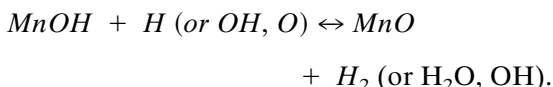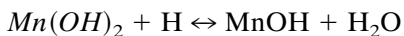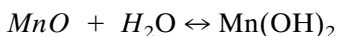
Fig. 9. First-order sensitivity coefficient of the burning velocity to the specific reaction rate constant for reactions with tin-containing species (1963 ppm of TMT).

The reaction pathway for manganese species is also shown in Fig. 8, and the pathway for iron species from $Fe(CO)_5$ is shown for comparison. As with iron pentacarbonyl, Mn reacts with O_2 to form MnO_2, which reacts primarily with radicals to form MnO. The catalytic radical recombination cycle consists of:

$$MnO + H_2O \leftrightarrow Mn(OH)_2$$

$$Mn(OH)_2 + H \leftrightarrow MnOH + H_2O$$

$$MnOH + H \ (or \ OH, O) \leftrightarrow MnO$$
$$+ \ H_2 \ (or \ H_2O, OH).$$

$net: H + H \leftrightarrow H_2$

$(or: H + OH \leftrightarrow H_2O)$

Although flame equilibrium calculations show that the species MnH is present at relatively large concentrations, the contribution of reactions of this species to the inhibition effect is relatively small. Figure 10 shows the highest absolute values of the sensitivity coefficients of

burning velocity to the rate constants (after adjustment) for reactions of manganese-containing species. The burning velocity is sensitive to the rates of the three reactions in the catalytic cycle above, with the rate of the reaction $Mn(OH)_2 + H \leftrightarrow MnOH + H_2O$ having the greatest absolute value. The burning velocity is also somewhat sensitive to the rates of the reactions forming MnO_2 and MnO. The reaction $MnO + H \leftrightarrow Mn + OH$ has a positive sensitivity; that is, increasing its rate increases the burning velocity. This chain propagating reaction temporarily removes MnO from the catalytic cycle above, thus weakening the inhibition.

Comparison of inhibition by $Fe(CO)_5$, MMT, and TMT

To evaluate the inhibition mechanisms under comparable conditions, the numerical calculations (for $\phi = 1.0$, $X_{O_2,ox} = 0.21$, and $T_{in} = 353$ K) were performed, as above, for initial values of TMT, MMT, and $Fe(CO)_5$ which provide an
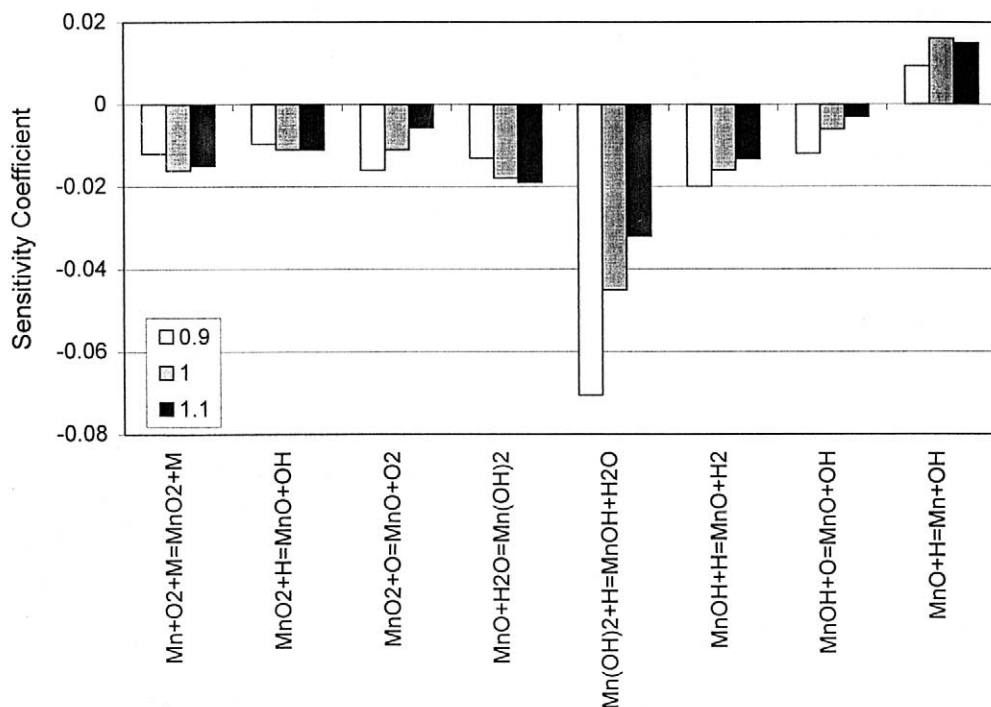
Fig. 10. First-order sensitivity coefficient of the burning velocity to the specific reaction rate constant for reactions with manganese-containing species (150 ppm of MMT).

equivalent reduction (30%) in the normalized burning velocity. These volume fractions were found to be 1963 ppm, 128 ppm, and 105 ppm, respectively. While suppression of a fire would probably require higher agent concentration than that which provides a 30% flame speed decrease, this degree of flame speed reduction was selected for two reasons. It provides a significant reduction in overall reaction rate (a factor of two), while keeping the agent concentration far enough above the values at which the model and experiments start to diverge (possibly because of condensation). For these flames, the structures are quite similar and the flame speed is the same (37.3 cm/s), allowing straightforward comparison of the inhibition mechanisms.

Based on the calculated results, TMT is required at a mole fraction which is about seventeen times greater than iron or manganese compounds for a similar reduction in overall reaction rate. This occurs because the reactions to form SnOH from SnO are rate limiting and slow. Further, the reverse of the reaction SnO +

H + M $\leftrightarrow$ SnOH + M is relatively fast at the location of peak catalytic cycle activity because SnO is a dominant equilibrium product in the high temperature region.

To further compare the performance of TMT, MMT, and $Fe(CO)_5$, it is useful to plot the relevant species mole fractions as a function of temperature through the flame. Figure 11 shows the mole fractions of the metal species in the inhibition cycles, and the radical species H, OH, and O. The vertical line shows the location of the maximum rate of the $H+O_2$ branching reaction. Note that the locations of the peak fluxes of the inhibition reactions are very close to the peak flux of the $H+O_2$ reaction and to the maximum concentrations H, OH, and O. The bottom figure for TMT inhibition clearly shows the preponderance of SnO as the sink for tin atoms (note the rescaling), hence requiring a large initial TMT mole fraction to achieve both fast reaction of SnO with H atom, and appreciable mole fraction of SnOH for radical scavenging. In Fig. 11, consider the manganese containing species at the location of peak H-
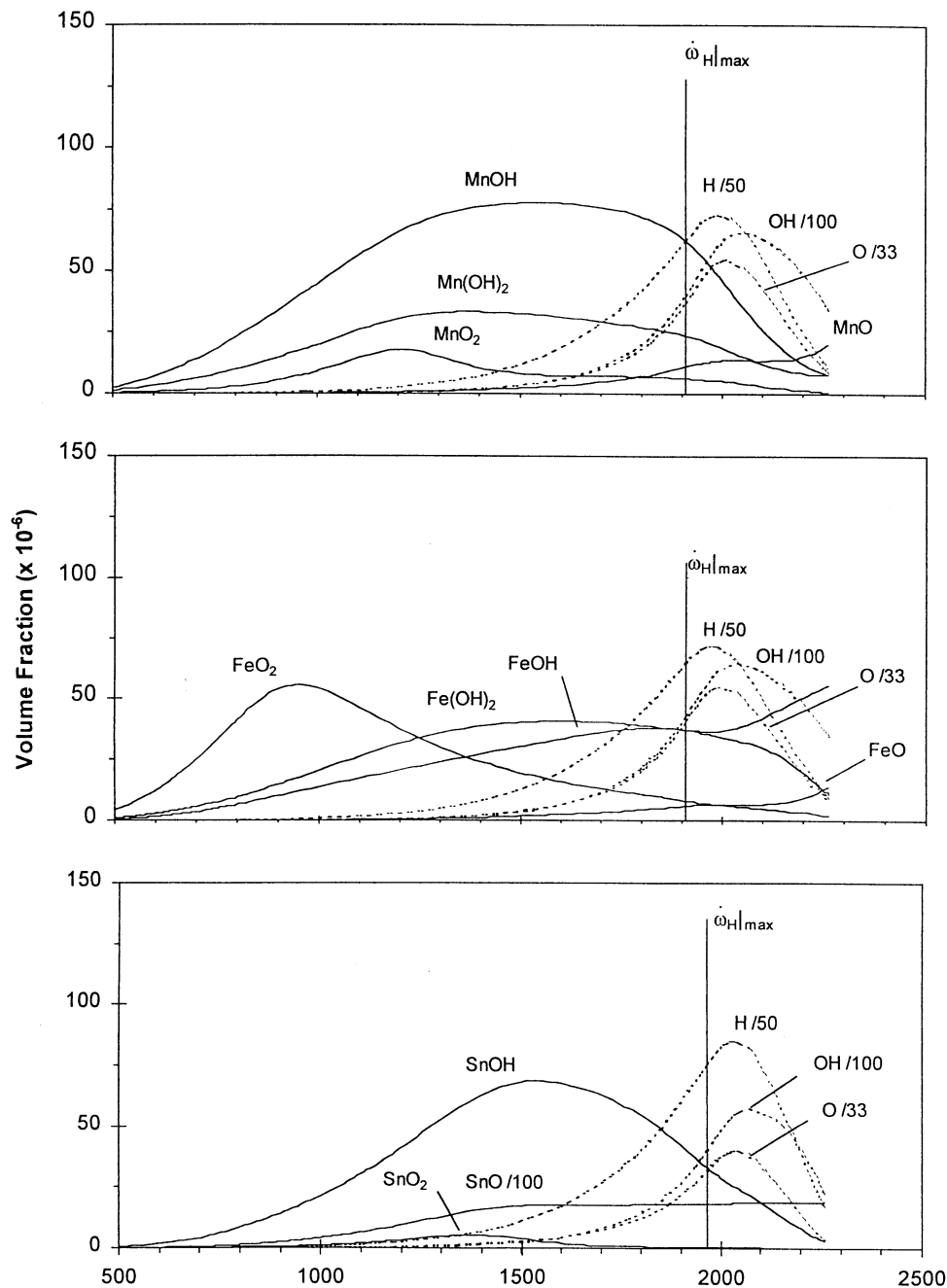
Fig. 11. Volume fraction of metal species intermediates and H, O, and OH radicals, as a function of temperature in flame for $Fe(CO)_5$, MMT, and TMT added at 106 ppm, 128 ppm, and 1963 ppm (corresponding to a 30% reduction in flame speed). T_{in} = 353 K, ϕ = 1.0, $X_{O_2,ox}$ = 0.21.

atom flux. MnO is present in higher mole fraction than FeO. This occurs from the significant backward reaction of $MnO + H_2O \leftrightarrow Mn(OH)_2$, which provides a lower $Mn(OH)_2$

concentration for the rate-limiting step $Mn(OH)_2 + H \leftrightarrow MnOH + H_2O$.

The importance of constraints on equilibrium concentrations as they relate to inhibitor effi-
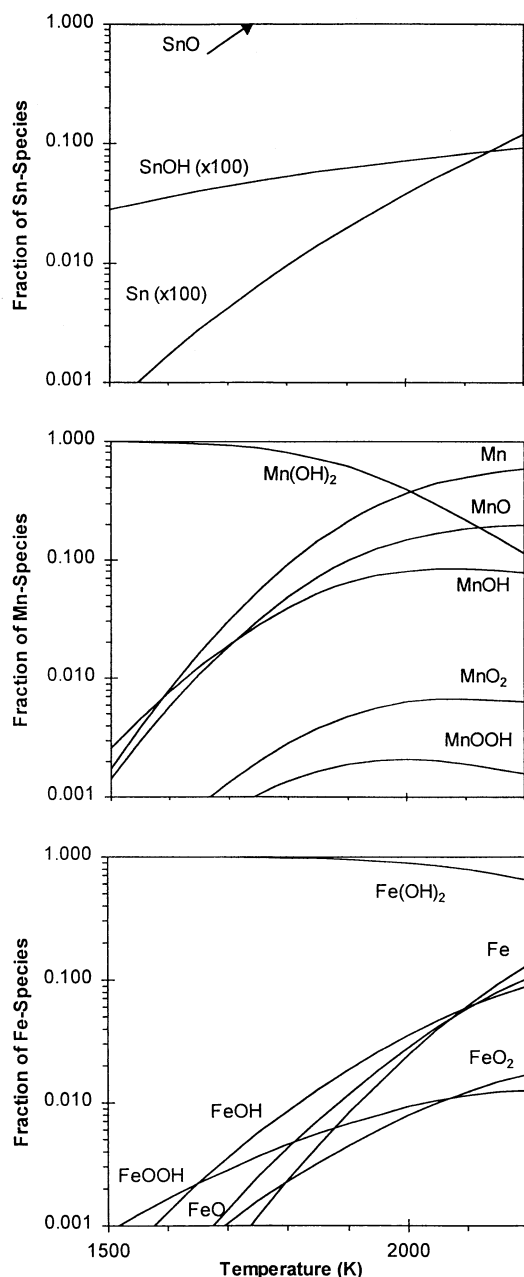
Fig. 12. Fraction of Sn-, Mn-, and Fe-species at equilibrium in methane-air flames as a function of temperature.

ciency is illustrated in Fig. 12 which shows the fraction of all metal species in the flame. For these equilibrium calculations, the metallic element (Sn, Mn, or Fe) is present at a mole fraction or 1.0×10^{-4}, and methane and air are present at stoichiometric proportions. For TMT inhibition, the Sn appears overwhelmingly as

SnO (note the scale change on Sn and SnOH), thus higher levels of TMT are necessary to yield the required levels of SnOH reaction with H atom, and for the required rates of the slow reaction $SnO + H + M \leftrightarrow SnOH + M$. Note that since the flames of Fig. 11 all have equivalent levels of inhibition, the flux of each radical recombining catalytic cycle is about the same; that is, SnOH, MnOH, and FeOH must be present at about the same mole fraction since their rates of reaction with H-atom are close, and the rates of reactions forming the hydroxide are approximately the same. Comparing $Mn(OH)_2$ and $Fe(OH)_2$ in Fig. 12, we see that in the MMT-inhibited flames, the concentration of $Mn(OH)_2$ for temperatures above 1800 K drops off rapidly, whereas in the $Fe(CO)_5$-inhibited flames, $Fe(OH)_2$ does not. Because the reaction of $Mn(OH)_2$ with H atom is rate-limiting (Fig. 10), decreases in the $Mn(OH)_2$ mole fraction make MMT less effective as an inhibitor than $Fe(CO)_5$.

CONCLUSIONS

In this work we presented the first experimental measurements of the influence of manganese- and tin-containing compounds (MMT, TMT) on the burning velocity of methane/air flames. Comparisons with the agents $Fe(CO)_5$ and CF_3Br demonstrate that manganese and tin-containing compounds are effective inhibitors. The inhibition efficiency of MMT is about a factor of two less than that of iron pentacarbonyl, and that of TMT is about twenty-six times less effective, although TMT is about twice as effective as CF_3Br. There exist conditions for which both MMT and TMT show a loss of effectiveness beyond that expected because of radical depletion, and the cause is believed to be particle formation. Kinetic models describing the inhibition mechanisms of MMT and TMT additives were suggested. Simulations of MMT- and TMT-inhibited flames show reasonable agreement with experimental burning velocity data. The decomposition of the parent molecule for the tin and manganese species is found to have a small effect on the inhibition properties for the range of concentrations used in this work. Calculations confirmed that the main

tin-containing species in the flame zone is SnO, while the concentrations of SnO_2, SnOH, and Sn are relatively small. The inhibition effect of TMT is determined mostly by the rate of the association reaction $H + SnO + M \leftrightarrow SnOH + M$, and the catalytic recombination cycle is completed by the reactions $SnOH + H \leftrightarrow SnO + H_2$ and $SnOH + OH \leftrightarrow SnO + H_2O$. The inhibition mechanism of manganese-containing compounds is similar, in many details, to the inhibition mechanism for iron pentacarbonyl: $MnO + H_2O \leftrightarrow Mn(OH)_2$; $Mn(OH)_2 + H \leftrightarrow MnOH + H_2O$, and $MnOH + OH$ (or H) $\leftrightarrow MnO + H_2O$ (or H_2). The burning velocity is most sensitive to the rate of $Mn(OH)_2 + H \leftrightarrow MnOH + H_2O$ reaction. Comparison of the mechanisms of inhibition of TMT and MMT to $Fe(CO)_5$ shows that the manganese is not as efficient an inhibitor as iron: because of equilibrium constraints, the mole fraction of the intermediate species $Mn(OH)_2$ drops off at higher temperature (in comparison to $Fe(OH)_2$, slowing its rate-limiting reaction with H atom in the catalytic cycle. This result illuminates the role of equilibrium constraints on species concentrations in the efficiency of catalytic cycles.

REFERENCES

1. Bulewicz, E. M., and Padley, P. J., *Proc. Combust. Inst.* 13:73 (1971).
2. Bulewicz, E. M., and Padley, P. J., *Chem. Phys. Lett.* 9:467 (1971).
3. Hastie, J. W., *High Temperature Vapors,* Academic Press, New York, 1975
4. Jensen, D. E., and Webb, B. C., *AIAA J.* 14:947 (1976).
5. Howard, J. B., and Kausch, W. J., *Prog. Energy Combust. Sci.* 6:263 (1980).
6. Cusack, P. A., and Killmeyer, A. J., *ACS Symp. Ser.* 425:189 (1990).
7. Hornsby, P. R., Mitchell, P. A., and Cusack, P. A., *Polym. Degrad. Stab.* 32:299 (1991).
8. Lask, G., and Wagner, H. G., *Proc. Combust. Inst.* 8:432 (1962).
9. Miller, D. R., Evers, R. L., and Skinner, G. B., *Combust. Flame* 7:137 (1963).
10. Miller, D. R., *Combust. Flame* 13:210 (1969).
11. Morrison, M. E., and Scheller, K., *Combust. Flame* 18:3 (1972).
12. Pitts, W. M., Nyden, M. R., Gann, R. G., Mallard, W. G., and Tsang, W., *Construction of an Exploratory List of Chemicals to Initiate the Search for Halon Alternatives,* National Institute of Standards and Technology, NIST Technical Note 1279, 1990.
13. Vanpee, M., and Shirodkar, P., *Proc. Combust. Inst.* 17:787 (1979).
14. Westblom, U., Fernandezalonso, F., Mahon, C. R., Smith, G. P., Jeffries, J. B., and Crosley, D. R., *Combust. Flame* 99:261 (1994).
15. Nesmeyanov, A. N. (Ed.), *Manganese Containing Antinock Compounds*, Nauka, Moskow, 1971.
16. Tapscott, R. E., Heinonen, E. W., and Brabson, G. D., *Advanced Agent Identification and preliminary Assessment*, NMERI, University of New Mexico, NMERI 95/38/32350, 1996
17. Chao, B. H., Egolfopoulos, F. N., and Law, C. K., *Combust. Flame* 109:620 (1997).
18. Andrews, G. E., and Bradley, D., *Combust. Flame* 18:133 (1972).
19. Linteris, G. T., and Truett, L., *Combust. Flame* 105:15 (1996).
20. Linteris, G. T., Rumminger, M. D., Babushok, V., and Tsang, W., *Proc. Combust. Inst.* 28:2965 (2000).
21. Rumminger, M. D., and Linteris, G. T., *Combust. Flame* 120:451 (2000).
22. Rumminger, M. D., and Linteris, G. T., *Combust. Flame* 123:82 (2000).
23. Rumminger, M. D., Reinelt, D., Babushok, V., and Linteris, G. T., *Halon Options Technical Working Conference*, Albuquerque, NM, 1998, pp. 145–156.
24. Gilbert, A. G., and Sulzmann, K. G. P., *J. Electrochem. Soc.* 121:832 (1974).
25. Stull, D. R., *Ind. Eng. Chem.* 39:517 (1947).
26. Hollrah, D., Ethyl Corp., Personal Communication, Jan. 2001
27. Bulewicz, E. M., and Padley, P. J., *Trans. Faraday Soc.* 67:2337 (1971).
28. Goodings, J. M., and Chen, Q.-F., *Can. J. Chem.* 76:1437 (1998).
29. Taylor, J. E., and Milazzo, T. S., *J. Phys. Chem.* 82:847 (1978).
30. Gurvich, L. V., Karachevtsev, G. V., Kondratiev, V. N., Lebedev, Yu. A., Medvedev, V. A., Potapov, V. K., and Hodeev, Ya. S., *Bond Energies. Ionization Potentials and Electron Affinities,* Nauka, Moskow, 1974.
31. Smith, G. P., Personal Communication, 1999.
32. Hildenbrand, D. L., and Lau, K. H., *J. Chem. Phys.* 100:8377 (1994).

33. Rumminger, M. D., Reinelt, D., Babushok, V., and Linteris, G. T., *Combust. Flame* 116:207 (1999).

34. Babushok, V., and Tsang, W., *Joint Meeting of the United States Sections of the Combustion Institute,* The Combustion Institute, Pittsburgh, PA, 1999, pp. 587–590.

35. Kee, R. J., Grcar, J. F., Smooke, M. D, and Miller, J. A., *A Fortran Computer Program for Modeling Steady Laminar One-dimensional Premixed Flames,* Sandia National Laboratories Report, SAND85-8240, 1991.

36. Kee, R. J., Rupley, F. M, and Miller, J. A., *CHEMKIN-II: A Fortran Chem. Kinetics Package for the Analysis of Gas Phase Chem. Kinetics,* Sandia National Laboratory, SAND89-8009B, 1989.

37. Kee, R. J., Dixon-Lewis, G., Warnatz, J., Coltrin, R. E, and Miller, J. A., *A Fortran Computer Package for the Evaluation of Gas-Phase, Multicomponent Transport Properties,* Sandia National Laboratory, SAND86-8246, 1986.

38. Smith, G. P., Golden, D. M., Frenklach, M., Moriarty, N. W., Eiteneer, B., Goldenberg, M., Bowman, C. T., Hanson, R. K., Song, S., Gardiner, Jr. W. C., Lissianski, V. V., and Qin, Z., http. //www.me.berkeley.edu/ gri mech, 2000.

39. Linteris, G. T., in *Halon Replacements* (A. W. Miziolek and W. Tsang, Eds.), Acs Symposium Series 611, Am. Chem. Society, Washington, DC, 1995.

40. Noto, T., Babushok, V., Hamins, A., and Tsang, W., *Combust. Flame* 112:147 (1998).

41. Linteris, G. T., Rumminger, M. D., and Babushok, V. I., *Combust. Flame* 122:58 (2000).

42. Fontijn, A., and Bajaj, P. N., *J. Phys. Chem.* 100:7085 (1996).

43. Husain, D., Plane, J. M., and Xiang, C. C., *J. Chem. Soc. Faraday Trans. 2* 80:1465 (1984).

44. Gurvich, L. V., Iorish, V. S., Chekhovskoi, D. V., Ivanisov, A. D., Proskurnev, A. Yu., Yungman, V. S., Medvedev, V. A., Veits, I. V., and Bergman, G. A., *IVTHANTHERMO—Database on Thermodynamic Properties of Individual Substances,* Institute of High Temperatures, Moscow, 1993.

45. Martinho Simões, J. A., in NIST Chemistry WebBook, NIST Standard Reference Database Number 69 (W. G. Mallard and P. J. Linstrom, Eds.), National Institute of Standards and Technology, Gaithersburg, MD 20899 (http. //webbook.nist.gov), 2000.

46. Lippincott, E. S., and Tobin, M. C. J., *J. Am. Chem. Soc.* 75:4141 (1953).

47. Jensen, D. E., *J. Chem. Soc. Faraday Trans.* 76:1494 (1980).